Supplemental Information

For the manuscript entitled:

"*Contextual responses drive a unique laminar signature in human V1*"

Jurjen Heij[1,2,3*], Luisa Raimondo[1,2,3], Jeroen C.W. Siero[1,2,4], Wietske van der Zwaag[1,2], Tomas Knapen[1,2,3], and Serge O. Dumoulin[1,2,3,5]

[1]Spinoza Centre for Neuroimaging, Amsterdam, Netherlands
[2]Department of Computational Cognitive Neuroscience and Neuroimaging, Netherlands Institute for Neuroscience, Amsterdam, Netherlands
[3]Department of Experimental and Applied Psychology, Vrije Universiteit Amsterdam, Amsterdam, Netherlands
[4]Department of Radiology, University Medical Center Utrecht, Utrecht, Netherlands
[5]Department of Experimental Psychology, Utrecht University, Amsterdam, Netherlands
[*]Correspondence: j.heij@herseninstituut.knaw.nl

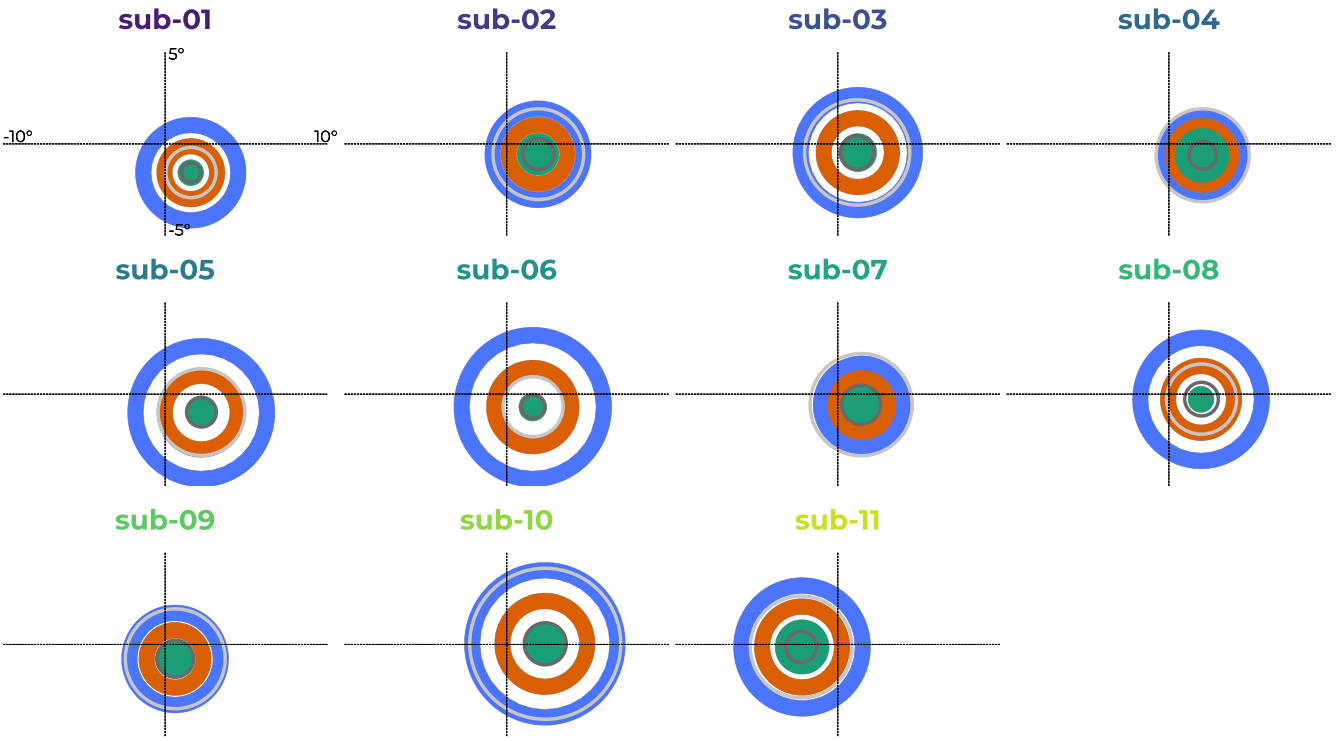

Figure S1: Participant-specific stimulus configurations as derived from computational modeling. The dark gray circle indicates the location of the full-width half-max of the spatial profile, whereas the light gray circle indicates the zero-crossing (Figure 2B). Most participants had the target pRF in the right hemifield which is encoded in the left hemisphere. This figure is related to Figure 2.

Table S1: Mixed-linear model regression results. We averaged the response over a time period around the peak of the response to the *center* stimulus (*intercept*) and entered this into a linear mixed-effects model. The medium annulus was defined as *suppr_1* and the large annulus as *suppr_2*. Post-hoc Tukey HSD pairwise comparisons further showed that response magnitude was significantly lower for the medium and large annulus compared to the center stimulus, while no significant difference was observed between the two annulus stimuli. These results highlight the effect of stimulus type on response magnitude, suggesting robust and consistent reductions in response during stimuli biased towards the normalization pool, with minimal variability across participants. The small residual variance (Scale=0.4405) and moderate random intercept variance (Group Var=0.059±0.05) further support the robustness of these results.

Model:	MixedLM	Dependent Variable:	gm
No. Observations:	330	Method:	REML
No. Groups:	11	Scale:	0.4405
Min. group size:	30	Log-Likelihood:	-345.0529
Max. group size:	30	Converged:	Yes
Mean group size:	30.0		

	Coef.	Std.Err.	z	P$>$ |z|	[0.025	0.975]
Intercept	1.473	0.097	15.243	0.000	1.284	1.663
event_type[T.suppr_1]	-1.275	0.089	-14.251	0.000	-1.451	-1.100
event_type[T.suppr_2]	-1.424	0.089	-15.917	0.000	-1.600	-1.249
Group Var	0.059	0.050				

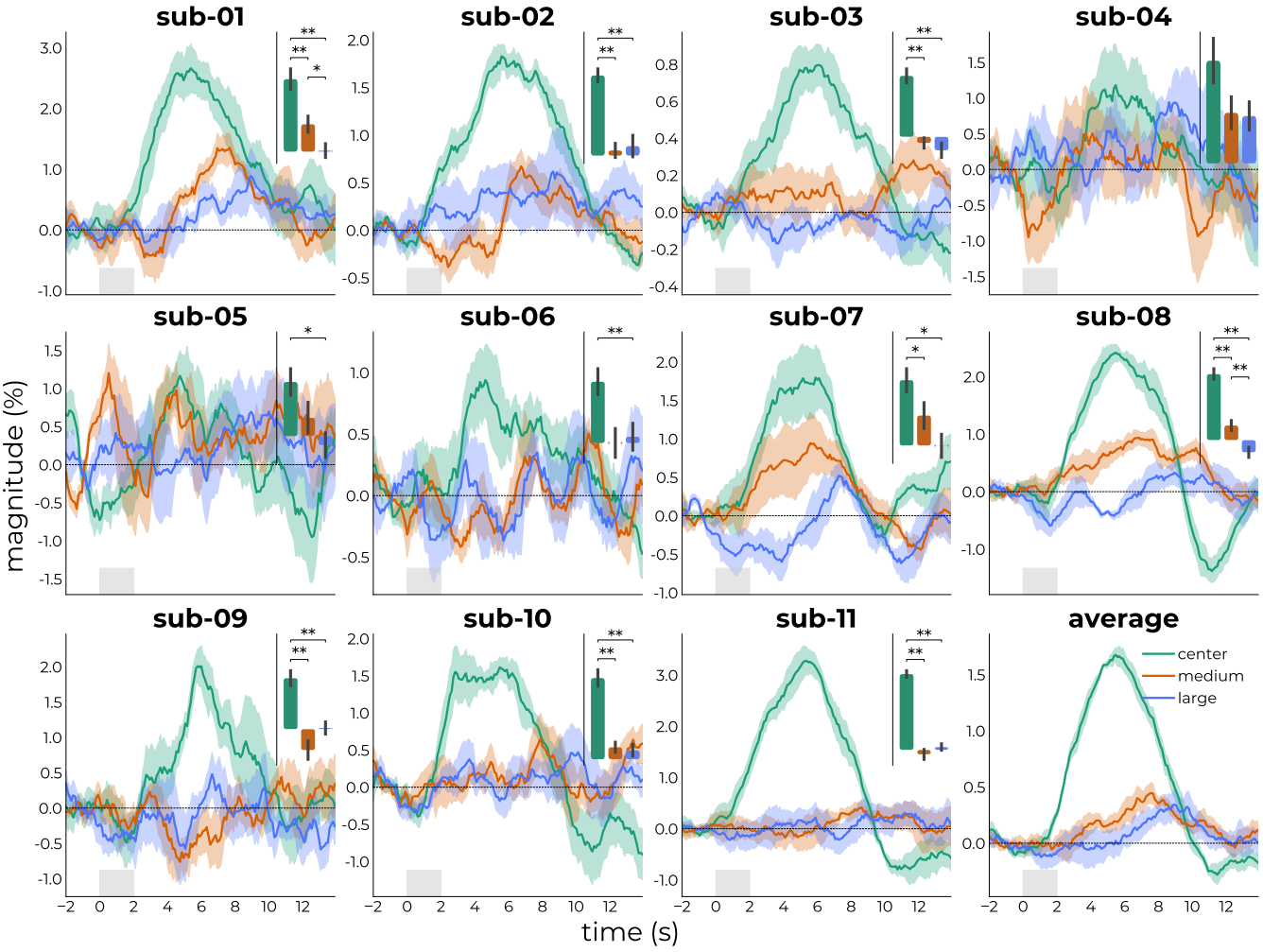

Figure S2: Participant-specific responses averaged across the cortical voxels to individually tailored stimuli. The bottom right panel represents the average across all participants. Insets represent participants-wise values extracted from the time point where the response to the *center*-stimulus peaked. Individual Friedman ANOVA's (as the data from some participants violated the normality assumption) were performed to formally test differences in response magnitude across stimulus types. Significance (asterisks) was based on post-hoc analyses using Wilcoxon signed-rank tests with Holm's correction. In all participants, the optimal stimulus (eliciting the largest response given the parameters of the pRF at the target location) according to the computational model resulted in the largest fMRI response in all participants (and reached significance in all but one participant). This figure is related to Figure 2D. *$p<0.05$, **$p<0.01$.

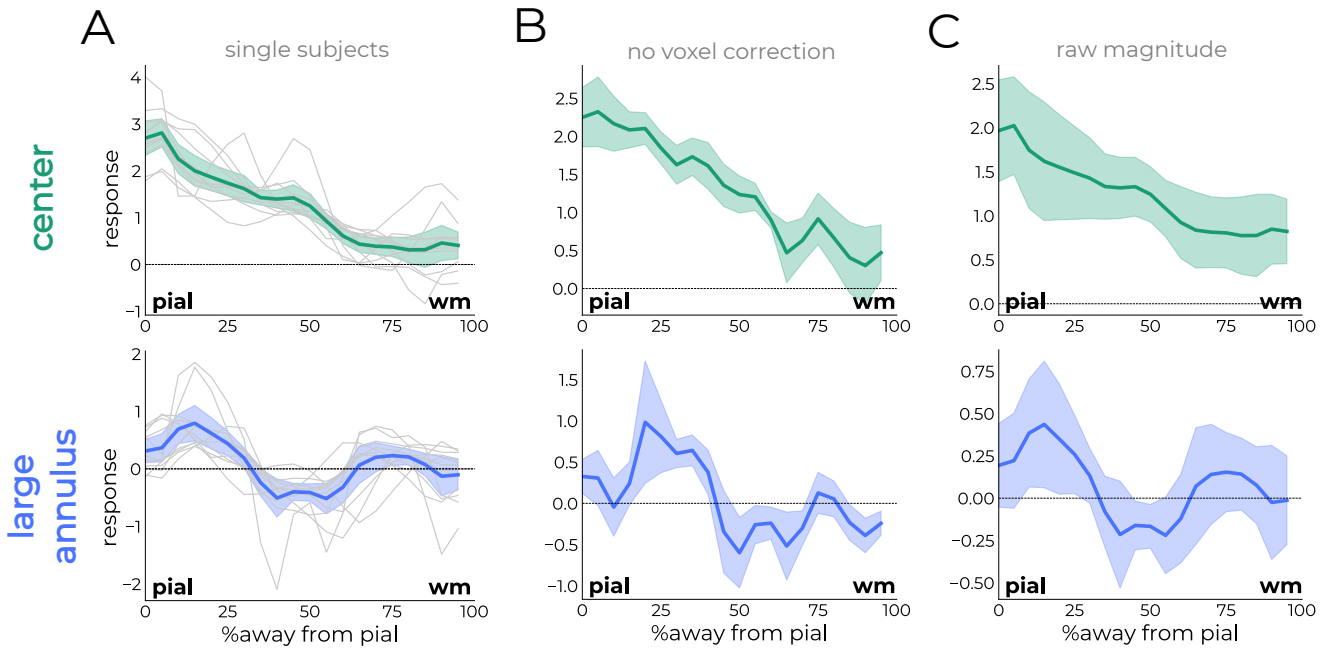

Figure S3: Control analyses. (A) Laminar results as shown in Figure 3, including participant-specific profiles. Although some variability between participants is observed, there is a remarkable consistency is localization of two peaks that align with termination sites of descending projection carrying feedback signals predicted from anatomical and electrophysiological work. (B) Response profiles of the dataset of included participants had the voxel correction approach not been applied (see also Figure S10). This led to a reduced number of participants, but the result remained clear. (C) Response profiles resulting from subject-specific magnitude responses (no normalization approach). This figure is related to Figure 3.

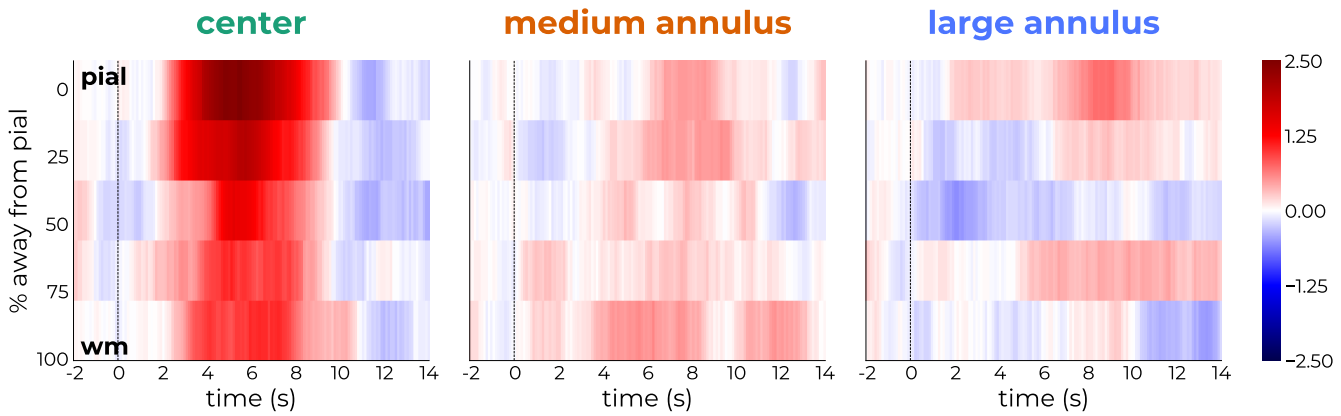

Figure S4: Laminar results without interpolation (related to Figure 4). Each participant's cortical column of interest was covered by 6–10 data points (voxels). In contrast to contemporary laminar studies that rely on interpolating 2–3 voxels to 20 depths (see refs[1–4]), line-scanning permits sampling many more data points across cortical depth. To synchronize the number of depths across participants, line-scanning uniquely allows averaging multiple voxels into a single compartment. In other words, the large number of data points allows for downsampling (averaging across multiple data points), rather than upsampling (expanding few data points into many). This boosts SNR without relying on interpolation. Using this approach, we could still observe the preference for signal processing in upper and deeper layers for stimuli targeting more of the normalization pool. The draining vein effect for center stimuli was also preserved. This figure is related to Figure 3.

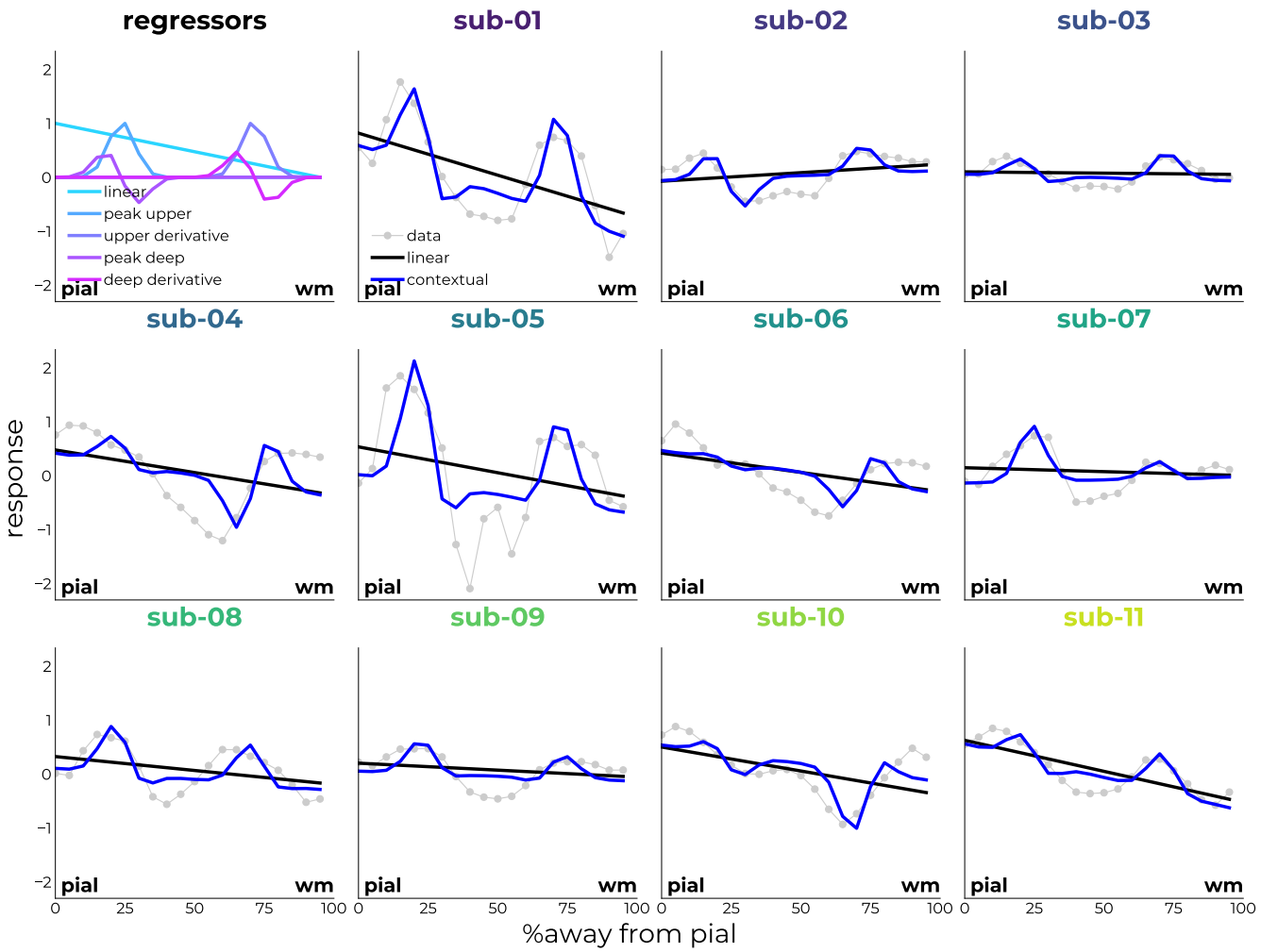

Figure S5: Participant-specific results of fitting the contextual model to cortical depth-dependent responses to the large annulus stimulus. The top-left panel represents the regressors entered into the model: a linear trend and two regressors and their derivatives (to allow shifts in exact location of the peaks) representing the termination sites of descending projections based on anatomical and functional studies. This figure is related to Figure 4.

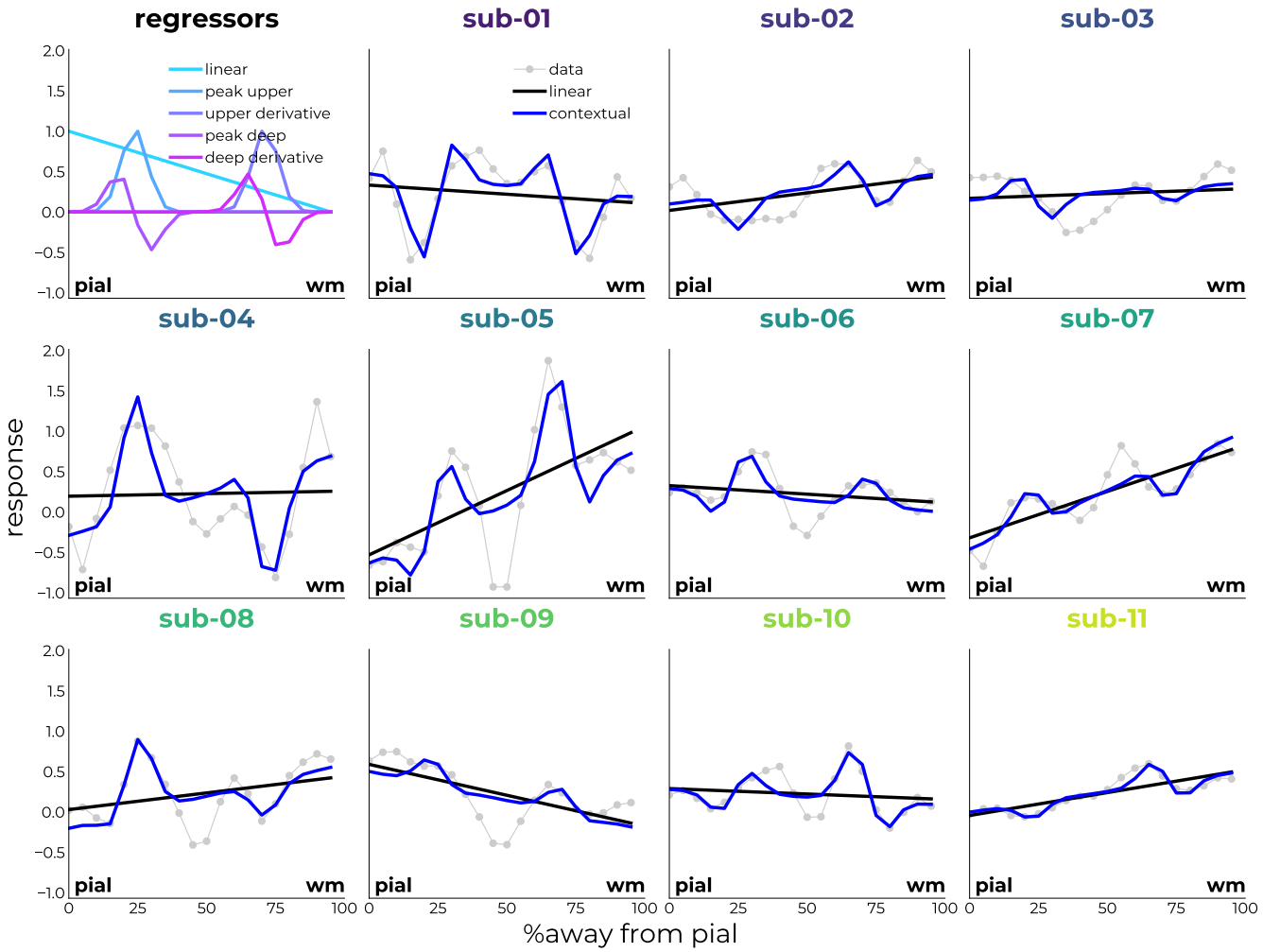

Figure S6: Participant-specific results of fitting the contextual model to cortical depth-dependent responses to the medium annulus stimulus. The same regressors as Figure S5 were used. This figure is related to Figure 6.

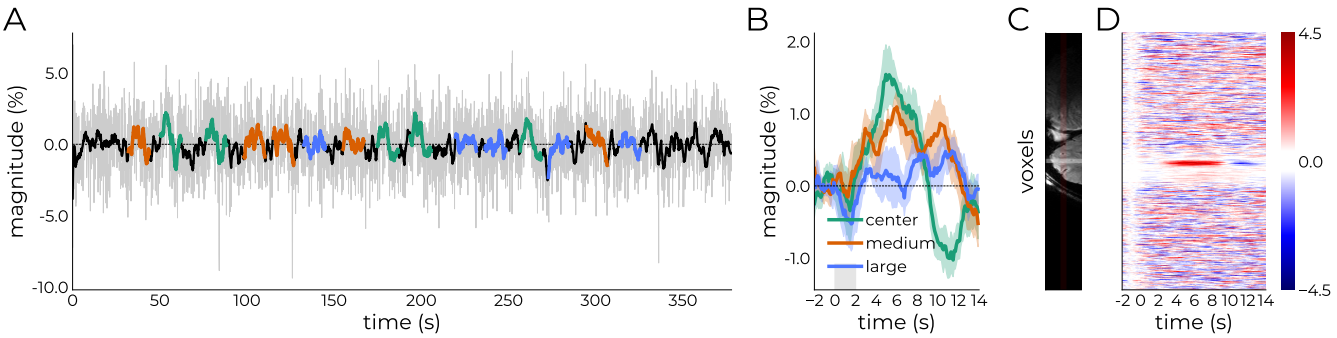

Figure S7: Epoching strategy and targeting success. (A) Example raw (light gray) and low-passed time course (black) or a single run with intervals around each respective stimulus onsets highlighted in their corresponding color (green = center, orange = medium annulus, and blue = large annulus). (B) Response profiles derived from averaging the epochs from all runs (shaded area represents ±SEM over the five epochs per event). (C) Section of anatomical reference slight with the gray shading representing the selected cortical ribbon. (D) Response evolution across the entire line, showing response preferences in the target location. This figure is related to the section "*Quantification and statistical analysis*".

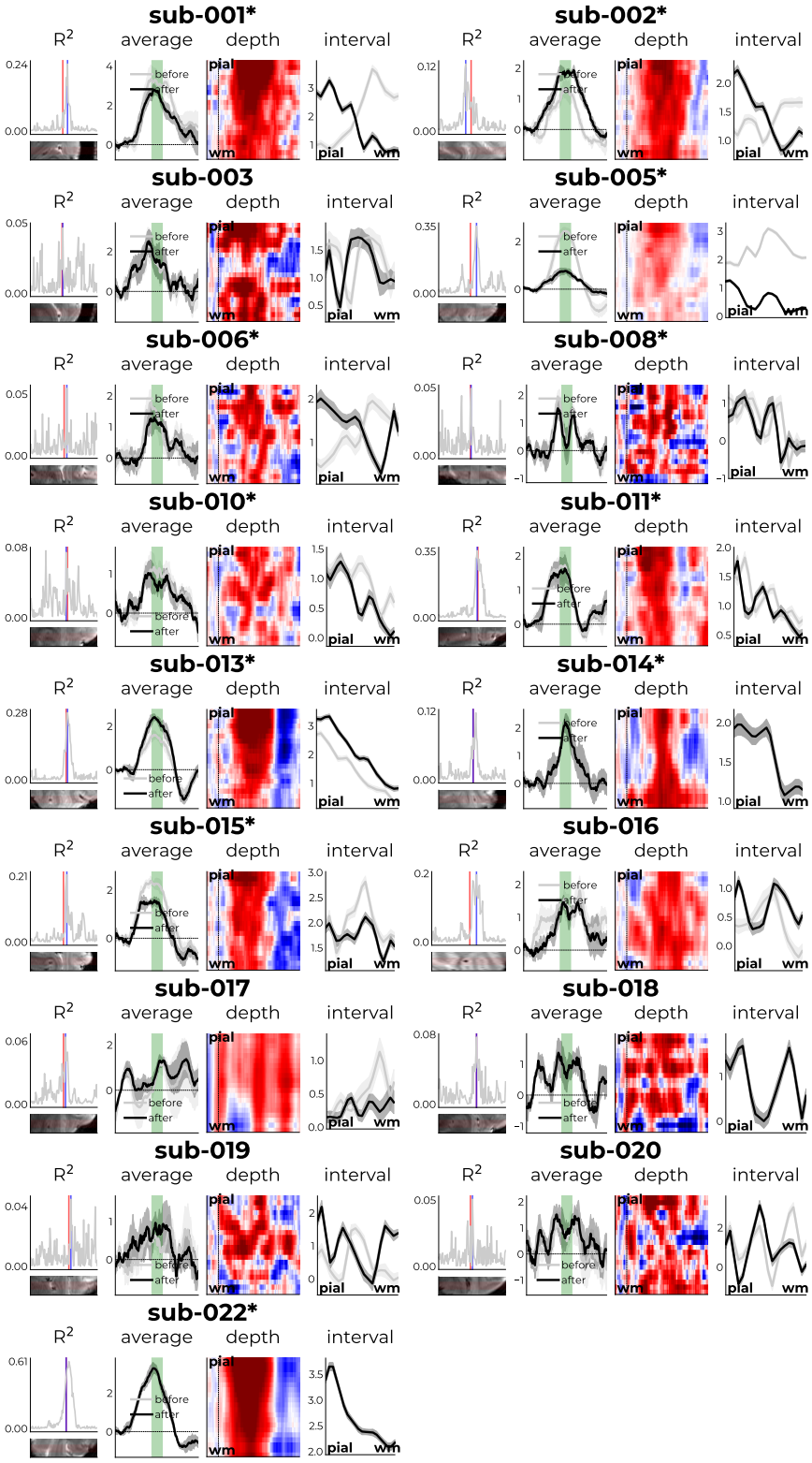

Figure S8: Voxel correction approach. First, a GLM model with the center event as reference was used to retrieve variance explained values across the line. Ideally, the variance explained should peak around the target coordinates (i.e., the middle of the line). To correct for small discrepancies between the anatomical voxel selection and functional acquisition (due to, e.g., motion), a correction was applied. Participants that passed both criteria are annotated with an asterisk (*). This figure is related to the section "*Quantification and statistical analysis*".

References

1. Huber, L., Finn, E. S., Chai, Y., Goebel, R., Stirnberg, R., Stöcker, T., Marrett, S., Uludag, K., Kim, S. G., Han, S. H., Bandettini, P. A., and Poser, B. A. (2021). Layer-dependent functional connectivity methods. Prog Neurobiol *207*, 101835. doi:10.1016/j.pneurobio.2020.101835.

2. Huber, L., Finn, E. S., Handwerker, D. A., Bönstrup, M., Glen, D. R., Kashyap, S., Ivanov, D., Petridou, N., Marrett, S., Goense, J., Poser, B. A., and Bandettini, P. A. (2020). Sub-millimeter fMRI reveals multiple topographical digit representations that form action maps in human motor cortex. NeuroImage *208*, 116463. doi:10.1016/j.neuroimage.2019.116463.

3. Huber, L., Handwerker, D. A., Jangraw, D. C., Chen, G., Hall, A., Stüber, C., Gonzalez-Castillo, J., Ivanov, D., Marrett, S., Guidi, M., Goense, J., Poser, B. A., and Bandettini, P. A. (2017). High-Resolution CBV-fMRI Allows Mapping of Laminar Activity and Connectivity of Cortical Input and Output in Human M1. Neuron *96*, 1253–1263.e7. doi:10.1016/j.neuron.2017.11.005.

4. Huber, L., Tse, D. H. Y., Wiggins, C. J., Uludağ, K., Kashyap, S., Jangraw, D. C., Bandettini, P. A., Poser, B. A., and Ivanov, D. (2018). Ultra-high resolution blood volume fMRI and BOLD fMRI in humans at 9.4 T: Capabilities and challenges. NeuroImage *178*, 769–779. doi:10.1016/j.neuroimage.2018.06.025.